



## Advances in concrete arch dams shape optimization

Jalal Akbari <sup>a,\*</sup>, Mohammad Taghi Ahmadi <sup>b</sup>, Hamid Moharrami <sup>b</sup>

<sup>a</sup>Department of Civil Engineering, Malayer University, Malayer, Iran

<sup>b</sup>Department of Civil Engineering, Tarbiat Modares University, Tehran, Iran

### ARTICLE INFO

#### Article history:

Received 10 January 2010

Received in revised form 17 December 2010

Accepted 11 January 2011

Available online 18 January 2011

#### Keywords:

Arch dam

Shape sensitivity analysis

Finite element modeling

Shape optimization

### ABSTRACT

This paper presents an efficient methodology to find the optimum shape of arch dams. In order to create the geometry of arch dams a new algorithm based on Hermit Splines is proposed. A finite element based shape sensitivity analysis for design-dependent loadings involving body force, hydrostatic pressure and earthquake loadings is implemented. The sensitivity analysis is performed using the concept of mesh design velocity. In order to consider the practical requirements in the optimization model such as construction stages, many geometrical and behavioral constraints are included in the model in comparison with previous researches. The optimization problem is solved via the sequential quadratic programming (SQP) method. The proposed methods are applied successfully to an Iranian arch dam, and good results are achieved. By using such methodology, efficient software for shape optimization of concrete arch dams for practical and reliable design now is available.

© 2011 Elsevier Inc. All rights reserved.

## 1. Introduction

Geometry has great influence in safety and economy of arch dams. Traditionally, shape design of an arch dam is based on the experience of the designer, model tests and trial and error procedures. To get a better shape, the designer should select several alternative schemes with various patterns and modify them to obtain a number of feasible shapes. The best shape considering the economy of design, structural considerations, safety, etc. is selected as the final shape. The shape of the dam obtained in this way is feasible but not necessarily optimum or even good. Moreover, the time of design is rather long. To overcome these difficulties, special efforts were begun by researchers for finding optimum shape of arch dams from the late 1960's.

Early research (Fialho and Serafim) [1,2] in this field, dealt with membrane-type solutions that ignored foundation elasticity and bending stresses, and considered a single, simple loading condition. Rajan [3], Mohr [4] and Sharma [5] considerably developed membrane shell theory based solutions. Sharpe [6] was the first one to formulate the optimization problem as a mathematical programming problem. A similar method was also adopted by Ricketts and Zienkiewicz [7] who used finite element method for stress analysis and Sequential Linear Programming (SLP) for the shape optimization of arch and buttress dams under static loads. Wassermann [8] used a mathematical formulation for arch dam design, in which the arch dam and part of its foundation were described by three-dimensional 8-node isoparametric hyper-elements. The optimization problem, was solved by SLP method. From other works in this field, the works done by Rahim [9], Samy [10], Yao and Choi [11], Guohua and Shuyu [12] can be mentioned. Fanelli and Salvaneschi [13] used the neural network approach to the definition of near optimal arch dam shape. Maher and Bidokhti [14] used simple genetic algorithm for finding optimum shape in their research. Salajegheh et al. [15] employed simultaneous perturbation stochastic approximation (SPSA) method to find optimum design. Arch dam optimization using a fuzzy inference system, wavelet neural network and grading

\* Corresponding author. Fax: +98 851 2221977.

E-mail addresses: [akbari@malayeru.ac.ir](mailto:akbari@malayeru.ac.ir) (J. Akbari), [mahmadi@modares.ac.ir](mailto:mahmadi@modares.ac.ir) (M.T. Ahmadi), [hamid@modares.ac.ir](mailto:hamid@modares.ac.ir) (H. Moharrami).

strategy is performed by Seyedpoor et al. [16,17]. Nevertheless, one of the most important investigations in this field was carried out by Bofang et al. [18–20] in China. It has been the basis of the majority of later works in the field of shape optimization of arch dams. From among the works done up to early 1990s in the field of shape optimization of concrete arch dams, the effects of seismic dynamic loads in the determination of the optimum shape of arch dams have rarely been considered. Bofang et al. considered dynamic loading in trial load method to optimize the shape of arch dams. Later, Simoes [21,22] continued his works using the finite element method for stress analysis for concrete gravity dams. In recent years, particular attention has been paid to this subject [23–25], where the number of articles in this field have been published in Chinese language [26,27]. Tajalli and Ahmadi [28] used Bofang formulation for parabolic arch dam. The finite element analysis and optimization procedure is implemented by commercial programs. Akbari And Ahmadi [29] optimized real double curvature parabolic arch dam with SQP method.

The gradient-based optimization algorithms need the derivatives of the constraints. Usually the derivatives are calculated via the overall finite difference methods, but the cost of computations for multiple loadings, especially in the earthquake loading is too expensive. In this paper, the finite element sensitivity based sensitivities are computed using the mesh design velocity [30]. The main advantage of this method is that, the sensitivities are independent of the step lengths.

In this investigation, the usual response spectrum method is used for seismic design of the arch dam. This research employs a new algorithm for geometry modeling of arch dams using Hermit cubic Splines. These Splines are useful for complicated valley shapes, especially those that have inflection points. In order to model accurate details, high numbers of design variables and constraints have been designated in the finite element and optimization models. For stress analysis, Extended Finite Element Analysis Program for Personal Version (EFEAPpv) has been modified.

In order to consider real construction conditions, multistage grouting, shear stresses in lift joints, stresses at separate cantilevers and minimum tensile stresses at monolithic body have been accounted in optimization procedure. Besides the main aim has been an attempt to develop the practical and professional software for shape optimization of arch dams with the acronym CADSO (Concrete Arch Dam Shape Optimization). The above methodologies have been successfully applied to the Karun IV arch dam in Iran. Obtained results from this study show that, shape optimization of that dam has the considerable reduction in the costs.

## 2. Dam geometry

### 2.1. Coordinate systems

The site geometry is defined in the fixed Cartesian system ( $x_s, y_s, z_s$ ). The axes  $x_s, y_s$  lie in a horizontal plane. The axis  $x_s$  is drawn to the right abutment and  $z_s$  vertically upward. The geometry of arch dam is described in the changeable Cartesian dam coordinate system with  $x_d, y_d, z_d, \theta_c$  design variables (Fig. 1). The coordinates are transformed between the site and the dam coordinate systems as:

$$\begin{bmatrix} x_s \\ y_s \\ z_s \end{bmatrix} = \begin{bmatrix} x_c \\ y_c \\ z_c \end{bmatrix} + \begin{bmatrix} \cos \theta_c & -\sin \theta_c & 0 \\ \sin \theta_c & \cos \theta_c & 0 \\ 0 & 0 & 1 \end{bmatrix} \begin{bmatrix} x_d \\ y_d \\ z_d \end{bmatrix}, \quad (1)$$

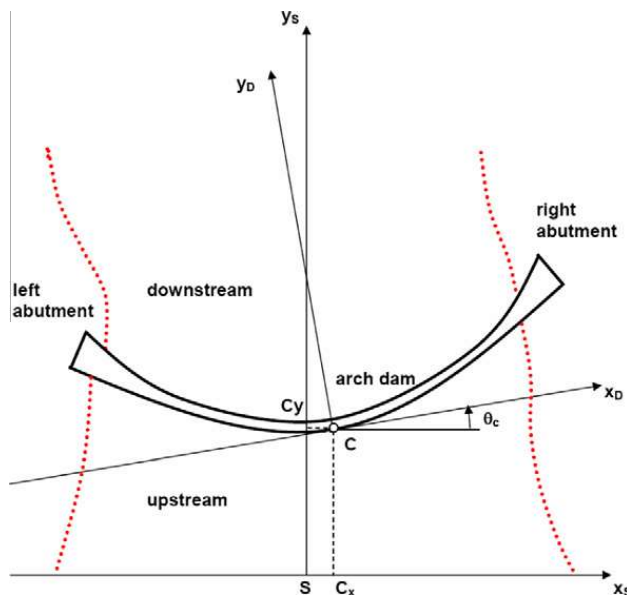


Fig. 1. Site and dam coordinate systems.

where subscript  $S$  is used for the site coordinate system,  $C$  for the origin of dam coordinate system and  $D$  for the coordinate of desired point in the dam system.

## 2.2. Crown cantilever shape

To define the geometry of the crown cantilever of an arch dam the eight design variables, including the crown thicknesses ( $T_b, T_m, T_u, T_c$ ) and the overhang parameters ( $p_b, p_m, p_u, p_c$ ), at the interpolation stations are needed (Fig. 2). The upstream and downstream faces of the crown are defined by the three pieces Hermit Spline as:

$$\begin{aligned} H_b : y_{u1} &= -P_b T_b, \quad y_{d1} = (1 - P_b) T_b, \\ H_m : y_{u2} &= -(1 + P_m) T_m, \quad y_{d2} = -P_m T_m, \\ H_u : y_{u3} &= -(1 + P_u) T_u, \quad y_{d3} = -P_u T_u, \\ H_c : y_{u4} &= 0, \quad y_{d4} = T_c. \end{aligned} \quad (2)$$

Here  $y_{ui}$  and  $y_{di}$  denote to the coordinates of interpolation nodes at upstream and downstream, respectively. The thickness of the crown ( $T$ ) at the desired level  $z$  is obtained as Eq. (3):

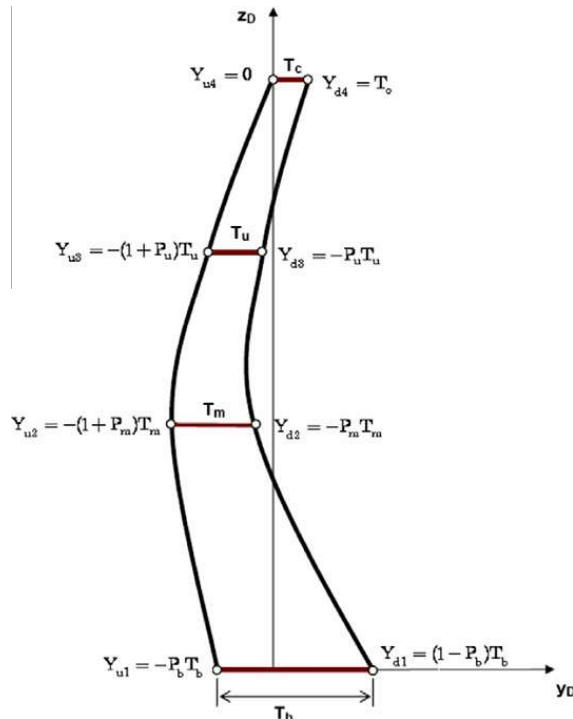
$$\begin{aligned} y_d &= \text{Spline}(z, y_{di}, H_i) : y_u = \text{Spline}(z, y_{ui}, H_i), \\ T &= y_d - y_u = \text{Spline}(z, y_{di}, H_i) - \text{Spline}(z, y_{ui}, H_i). \end{aligned} \quad (3)$$

## 2.3. Thickness of the dam body

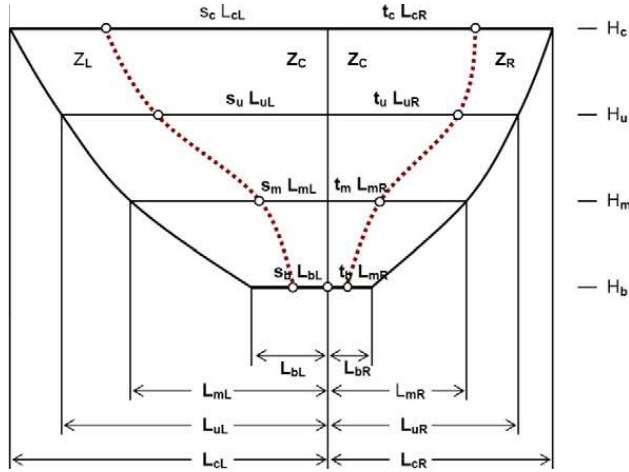
The thickness of a crown cantilever is specified by the  $T_b, T_m, T_u, T_c$  design variables. The upstream face of a dam is divided into a central zone, which will be denoted by  $Z_C$  and the zones of variable thicknesses at the left and right abutments, which will be defined by  $Z_L$  and  $Z_R$  (Fig. 3). In  $Z_C$  the thickness of the dam body in the desired level equals with thickness in the crown joint. In  $Z_L$  and  $Z_R$ , the thickness in the needed level varies parabolically from the thickness at  $Z_C$  to the thickness at the abutments. The starting points of the thickness variable zones in the interpolation stations at right and left are defined by eight  $t_b, t_m, t_u, t_c$  and  $s_b, s_m, s_u, s_c$  design variables. As well, the thickness of the dam body at the right and left abutments is specified by  $T_{rb}, T_{rm}, T_{ru}, T_{rc}$  and  $T_{lb}, T_{lm}, T_{lu}, T_{lc}$  design variables. The thickness of abutment is interpolated by the cubic Hermite Splines over the dam height.

$$T_{aR} = \text{Spline}(z, T_{iR}, H_i) : T_{aL} = \text{Spline}(z, T_{iL}, H_i). \quad (4)$$

In order to compute the central zone widths at the reference levels, dam widths at these levels are determined by finding the intersection of the upstream horizon with the sound rock. The  $x_D$  coordinates of the intersection points are denoted by  $L_{iR}, L_{iL}$



**Fig. 2.** The crown cantilever profile and the reference levels.

**Fig. 3.** The thickness zones of the dam body.

(Fig. 3). The central zone widths are determined from the dam widths and the starting variable thickness points  $t_i, s_i$ . The zone widths at the desired level are calculated with the Splines as:

$$\bar{R}_i = t_i L_{iR}, \quad \bar{L}_i = s_i L_{iL}, \quad (5)$$

$$L_{\text{Right}} = \text{Spline}(z, \bar{R}_i, H_i) : L_{\text{Left}} = \text{Spline}(z, \bar{L}_i, H_i). \quad (6)$$

#### 2.4. Shape of elevation arches

As mentioned in (2.3), each elevation has two thickness zones. For the desired level  $z$  as shown in Fig. 4, the upstream equation corresponds to a parabola whose vertex lies on the upstream edge of the crown cantilever crest. The parabola radius curvature ( $r$ ) at the interpolation points represented by the  $R_b, R_m, R_u, R_c$  design variables.  $r$  is interpolated between these levels by the following equation:

$$r = \text{Spline}(z, H_i, R_i). \quad (7)$$

The equation of the parabola  $AB$  with vertex  $(a_x, a_y)$  and radius  $r$  is as Eq. (8):

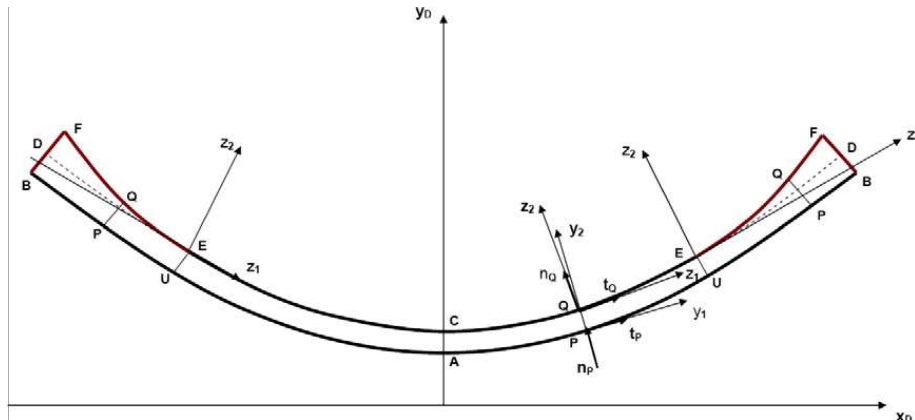
$$y = a_y + \frac{1}{2r} (x - a_x)^2 : \frac{dy}{dx} = \frac{x - a_x}{r} = \alpha. \quad (8)$$

Consider a point  $P$  on the curve  $AB$ . The unit normal and tangent vectors  $\mathbf{n}_P, \mathbf{t}_P$  at point  $P$  are:

$$\mathbf{n}_P = \begin{bmatrix} n_x \\ n_y \end{bmatrix}_P = \begin{bmatrix} -t_y \\ t_x \end{bmatrix}, \quad \mathbf{t}_P = \begin{bmatrix} t_x \\ t_y \end{bmatrix}_P = \begin{bmatrix} \frac{1}{\sqrt{1+\alpha^2}} & \frac{\alpha}{\sqrt{1+\alpha^2}} \end{bmatrix}^T. \quad (9)$$

The curve  $CD$  is derived from parabola  $AB$  so that the thickness  $T$  in the direction of the normal  $\mathbf{n}_P$  be constant. Construct a local coordinate system  $z_1, z_2$  with base  $\mathbf{n}_P, \mathbf{t}_P$ , at point  $P$ . The axis  $z_2$  intersects the curve  $CD$  in  $Q$ :

$$\mathbf{X}_Q = \mathbf{X}_P + T \mathbf{n}. \quad (10)$$

**Fig. 4.** An elevation arch of the dam body.

The derivative of the curve  $CD$  is as Eq. (11):

$$\beta = \frac{dy_Q}{dx} = \frac{dy_p}{dx} + T \frac{dn_y}{dx} = \alpha \left( 1 - \frac{T}{r} (1 + \alpha^2)^{-1.5} \right). \quad (11)$$

The unit tangent and normal vectors  $\mathbf{t}_Q, \mathbf{n}_Q$  to the curve  $CD$  at point  $Q$  are as Eq. (12):

$$\mathbf{n}_Q = \begin{bmatrix} n_x \\ n_y \end{bmatrix}_Q = \begin{bmatrix} -t_y \\ t_x \end{bmatrix}_Q, \quad \mathbf{t}_Q = \begin{bmatrix} t_x \\ t_y \end{bmatrix}_Q = \begin{bmatrix} \frac{1}{\sqrt{1+\beta^2}} & \frac{\beta}{\sqrt{1+\beta^2}} \end{bmatrix}^T. \quad (12)$$

According to Fig. 4, the arch thicknesses vary from  $T$  at point  $U$  to  $T_a$  at the end point  $B$  of the parabola. Let curve  $EF$  be a parabola with vertex  $E$  which is tangential to curve  $CD$  at point  $E$ . Its radius of curvature ( $r_E$ ) is chosen so that the parabola passes through point  $F$ ,

$$z_2 = \frac{1}{2r_E} z_1^2 : r_E = \frac{z_{1F}^2}{2z_{2F}} \rightarrow z_2 = z_{2F} \left( \frac{z_1}{z_{1F}} \right)^2, \quad (13)$$

$$\mathbf{X}_F = \mathbf{X}_B + T_a \mathbf{n}_B :: \mathbf{Z}_F = \mathbf{R}_E^T (\mathbf{X}_B - \mathbf{X}_E + T_a \mathbf{n}_B) :: \mathbf{R}_E = \begin{bmatrix} t_x & n_x \\ t_y & n_y \end{bmatrix}_E. \quad (14)$$

In which  $z_{1F}, z_{2F}$  are local coordinates of the point  $F$ .  $\mathbf{Z}_F^T = [z_{1F} \ z_{2F}]$  is determined relative to the  $B$  so that the thickness of the dam normal to the upstream face at the abutment equals  $T_a$ . Therefore  $\mathbf{Z}_F$  is determined by Eq. (14). Consider a point  $P$  on the parabola  $AB$  in the variable thickness zone  $EF$  in Fig. 4. The unit normal  $\mathbf{n}_P$  to  $AB$  at  $P$  cuts the downstream parabola  $EF$  in  $Q$ . The coordinate of  $Q$  in the dam coordinate system is determined as:

$$\mathbf{X}_Q = \mathbf{X}_P + \bar{T} \mathbf{n}_P, \quad (15)$$

where  $\bar{T}$  is thickness of desired point in the variable thickness zone. The coordinate of  $Q$  is

$$\mathbf{X}_E + \mathbf{R}_E \mathbf{Z}_Q = \mathbf{X}_P + \bar{T} \mathbf{n}_P. \quad (16)$$

$\bar{T}$  is eliminated from Eq. (16) with scalar product by  $\mathbf{t}_P$

$$\begin{aligned} \mathbf{t}_P^T \mathbf{X}_E + \mathbf{t}_P^T \mathbf{R}_E \mathbf{Z}_Q &= \mathbf{t}_P^T \mathbf{X}_P \rightarrow \frac{\bar{B}}{2r_E} z_{1Q}^2 + \bar{A} z_{2Q} + \bar{C} = 0, \\ \bar{A} &= t_{xp} r_{11} + t_{yp} r_{21} : \bar{B} = t_{xp} r_{12} + t_{yp} r_{22} : \bar{C} = t_P^T (\mathbf{X}_E - \mathbf{X}_P). \end{aligned} \quad (17)$$

Substituting the local coordinate  $Z_1$  from Eq. (14) the Eq. (18) is obtained.

$$\frac{\bar{B}}{2r_E} z_1^2 + \bar{A} z_2 + \bar{C} = 0 : z_2 = \frac{z_1^2}{2r_E} : \mathbf{X}_Q = \mathbf{X}_E + \mathbf{R}_E \mathbf{Z}_Q \rightarrow \bar{T} = \mathbf{n}_P^T (\mathbf{X}_Q - \mathbf{X}_P). \quad (18)$$

Thickness of a arch in the variable thickness zone is determined by Eq. (18). The points  $B$  and  $H$  in Fig. 5 are the intersection points of the upstream and downstream parabolas with the sound rock. The location of point  $F$  in the downstream edge is determined so that it lies on the normal  $\mathbf{n}_B$  to the upstream edge. For determining final contact line  $GH$ , the difference in the  $x_0$  coordinates of points  $G$  and  $B$  is set equal to the difference in the  $x_0$  coordinates of points  $H$  and  $F$ . The coordinate  $x_1$  of point  $G$  is determined so that it lies on the extended parabola  $AB$ . The location of the transition points  $E$  and  $U$  between the zones of constant and variable thickness is not changed in the specified elevation.

$$x_G = x_B + (x_H - x_F); \quad y_G = a_y + \frac{1}{2r} x_G^2. \quad (19)$$

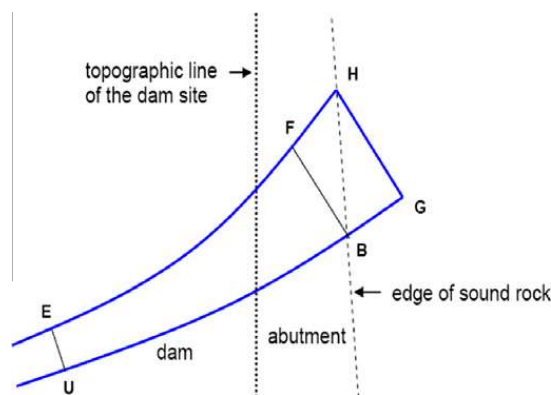


Fig. 5. Contact line between elevation and abutment.

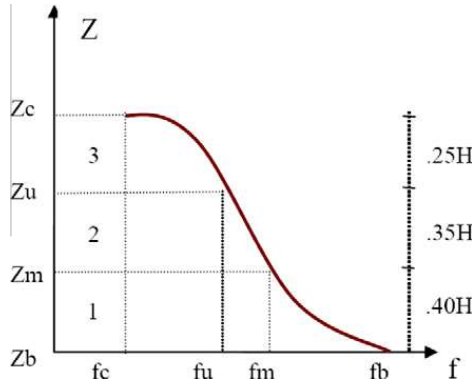


Fig. 6. Hermit Splines Interpolation.

## 2.5. Hermit cubic Splines

Assume the value of the unknown parameter i.e.  $(f)$  in the desired  $z$  is required. In Fig. 6, the known values of  $(f)$  in the interpolation stations are denoted by  $f_b, f_m, f_u, f_c$ .

The Hermit Splines pass through from the interpolation stations. The value of  $(f)$  at the desired levels is calculated as:

$$\begin{aligned} \mathbf{f} &= \mathbf{Q}\bar{\mathbf{f}}^T, \\ \mathbf{Q} &= \{Q_1, Q_2, Q_3, Q_4\}, \quad \bar{\mathbf{f}} = \{f_i, h_i f'_i, f_{i+1}, h_i f'_{i+1}\}, \\ Q_1 &= 2 - 3\xi + \xi^3, \quad Q_2 = 1 - \xi - \xi^2 + \xi^3, \quad Q_3 = 2 + 3\xi - \xi^3, \quad Q_4 = -1 - \xi + \xi^2 + \xi^3, \end{aligned} \quad (20)$$

where  $-1 \leq \xi \leq 1$  is the normalized values of the  $z$  with respect to  $H$ . The values of  $f'_i$  in the each segment of Splines are calculated by Eq. (21):

$$\begin{bmatrix} f'_b \\ f'_m \\ f'_u \\ f'_c \end{bmatrix} = \begin{bmatrix} \frac{4315}{1342} & \frac{40125}{9394} & \frac{-6528}{4697} & \frac{224}{671} \\ \frac{-1435}{1342} & \frac{-9795}{9394} & \frac{13056}{4697} & \frac{-448}{671} \\ \frac{175}{671} & \frac{-8625}{4697} & \frac{-2988}{4697} & \frac{1484}{671} \\ \frac{-175}{1342} & \frac{8625}{9394} & \frac{-26688}{4697} & \frac{3284}{671} \end{bmatrix} \begin{bmatrix} \frac{f_b}{H} \\ \frac{f_m}{H} \\ \frac{f_u}{H} \\ \frac{f_c}{H} \end{bmatrix}. \quad (21)$$

Then the value of  $(f)$  at each piece of Splines, is computed in the desired  $z$  with Eq. (22):

$$\begin{aligned} f(z) &= \frac{1}{4} [Q_1 f_i + Q_2 h_i f'_i + Q_3 f_{i+1} + Q_4 h_i f'_{i+1}], \\ h_1 &= 0.200H, \quad h_2 = 0.175H, \quad h_3 = 0.125H. \end{aligned} \quad (22)$$

With the above steps and defined design variables, the three-dimensional finite element model of the system is created. Typical shape of the system is presented in Fig. 7. A full definition of the design variables set is introduced in the Section 5.1.

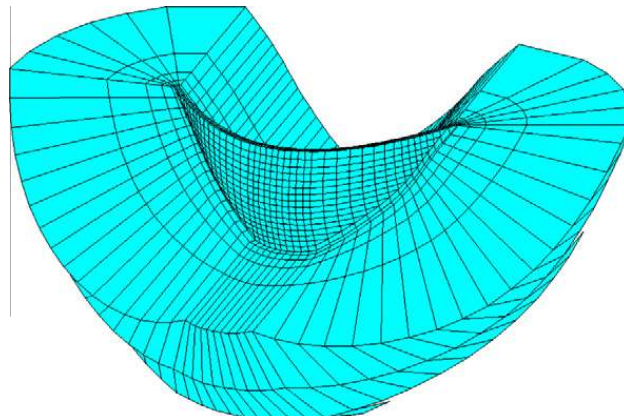


Fig. 7. Three-dimensional shape of the dam and its foundation.

### 3. Finite element model

#### 3.1. Finite element mesh and loadings

Only the dam and foundation meshes, as illustrated in Fig. 7, are used. The foundation mesh extension in horizontal directions is about the dam height at crest elevation, whereas at the dam bottom it is extended 1.5 times the dam height deep into the rock. The reservoir dynamic effect has been approximated by the added mass concept. All the elements used are linear solid. Four layers of these are used across the dam body thickness. Three basic loading cases (i.e. gravity, static dominant, and dynamic) have been considered in this research. For each case, separate mesh generation has been considered for finite element analysis. The requirements of these loading cases have to be satisfied simultaneously for a single shape optimization process.

##### 3.1.1. Gravity loadings

This load is applied to the free separate portions of cantilevers (where non-grouted) and to the monolithic shell structure (where grouted). Thus, for the dead load case, sequentially variable meshes are generated for any desired number of grouting stages. If it is assumed the user selects a three-stage grouting course, in the first stage two sets of odd and even cantilever meshes are generated from the base to the elevation  $H/3$  for the stress analysis of the free separate cantilevers. For the second stage of construction, the dam body is modelled from the base to elevation. The lower third of the dam is grouted (and thus is now a monolithic shell), and the remaining upper part comprises of free cantilevers (i.e. even and odd separate cantilevers) and thus the model is analyzed for stress calculation. In the last stage, the entire body of the dam is modelled. Now the lower two-third part of the dam is grouted (thus is a monolithic shell), and the upper third part is modelled for stress analysis of free cantilevers. At each construction stage, the stresses of the previous stages are added up to the stresses induced by the free separate upper portion of cantilevers. Thereafter, the entire structure is assumed as a monolithic shell and ready for bearing other static and dynamic loads. This loading shall be referred to as loading case 1.

##### 3.1.2. Static loadings

Monolithic shell structure of a dam body is subjected to the action of a full reservoir hydrostatic pressure plus the gravity load. In this paper, hydrostatic load is computed automatically in the upstream face of the dam body. This loading shall be considered as loading case 2.

##### 3.1.3. Seismic loadings

The loading case 2 is superposed by the effects of longitudinal component of the Operating Basis Earthquake (OBE) defined by a target spectrum. The seismic load level adopted corresponds to the medium (OBL) not the significant level (MDL or MCL) of ground motion. Because we optimize the shape for rather high probability loads not very low probability loads, so in this loading level linear solution is valid for finite element analysis. At (DBL), the nonlinearity phenomenon is not activated in general. Once the design is done, nonlinear behaviors (such as joint opening, crack growth, etc.) consequence under an extreme seismic load only has to be checked to ensure safety. Indeed, it is believed that if optimal design under the DBL seismic load is achieved the extreme condition is relieved to some extent. So arch dams shape optimization under dynamic seismic load with linear behavior is common in dam engineering. Using the response spectrum method, the maximum nodal displacements and element stresses are computed separately for each individual mode of vibration and are then combined to obtain the total maximum response values due to the first 15 modes of vibration. Damping ratio is considered equal to (5%). The CQCmodal combination method is used for combination of modal response.

### 4. Sensitivity analysis

#### 4.1. Mesh design velocity

As explained in the Section 2, a group of the shape design variables ( $\mathbf{X}$ ) are defined in order to change the geometry of the structure. The concept of mesh design velocity ( $\mathbf{V}$ ), which represents the changes of finite element nodal coordinates for a given shape design variable, could be used for this purpose to achieve high computational efficiencies [31]. By introducing a scalar parameter,  $\tau$ , which control the magnitude of the design change, the mesh design velocity  $\mathbf{V}$  as shown in Fig. 8, can be obtained as in Eq. (23):

$$\mathbf{V}(x, y, z) = \frac{(\mathbf{X}_{\text{new}} - \mathbf{X}_{\text{old}})}{\tau}, \quad (23)$$

where  $\mathbf{X} = X(x, y, z)$ ,  $\mathbf{X}_{\text{new}}$ ,  $\mathbf{X}_{\text{old}}$  are the perturbed and original finite element nodal coordinates, respectively. In the shape optimization problems the derivatives calculations are very tedious. However, using the latter concept, these derivatives are efficiently available.

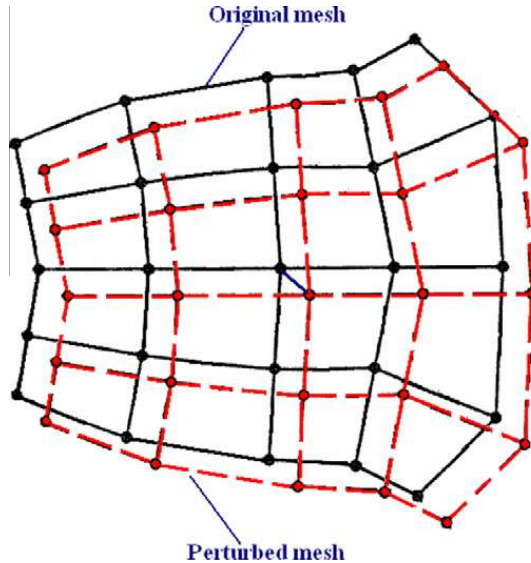


**Fig. 8.** The schematic shape of 2D finite element mesh using linear mapping (without supports).

The finite element static equilibrium equation for solid mechanics is processed as Eq. (24):

$$\mathbf{KU} = \mathbf{P},$$

$$\mathbf{K} \frac{\partial \mathbf{U}}{\partial \mathbf{X}} = \frac{\partial \mathbf{P}}{\partial \mathbf{X}} - \frac{\partial \mathbf{K}}{\partial \mathbf{X}} \mathbf{U} = \sum_{e=1}^{ne} \left( \frac{\partial \mathbf{p}_e}{\partial \mathbf{X}} - \frac{\partial \mathbf{k}_e}{\partial \mathbf{X}} \mathbf{u} \right). \quad (24)$$

In which  $\mathbf{P} = \mathbf{P}_b + \mathbf{P}_s$  and  $\mathbf{P}_b, \mathbf{P}_s$  are gravity and traction loads, respectively.

#### 4.2. Body force derivatives

In the finite element method, the body force loads and their sensitivities are as following:

$$\mathbf{P}_b^e = \int_{\Omega} \mathbf{N}^T \mathbf{b} d\Omega = \sum_{i=1}^{Nquad} w_i \mathbf{N}^T \mathbf{b} |\mathbf{J}| \rightarrow \mathbf{P}_b^e = \sum_{i=1}^{Nquad} w_i \mathbf{N}^T \mathbf{b} |\mathbf{J}'|. \quad (25)$$

$\mathbf{b} = \{\gamma_x, \gamma_y, \gamma_z\}$  is the body force and is independent of the shape variables. Therefore, In Eq. (25) the value of  $\mathbf{b}'$  is zero. The gradients of the body forces are related only to the derivatives of the determinate of the  $\mathbf{J}$  matrix. The  $|\mathbf{J}'|$  is calculated as follows wherein necessarily  $|\mathbf{J}'| \neq |\mathbf{J}|$ :

$$\mathbf{J} = \left[ \frac{\partial \mathbf{x}}{\partial \mathbf{r}} \right] = \left[ \sum_{i=1}^{nen} \frac{\partial N_i}{\partial \mathbf{r}} \mathbf{x}_i \right], \quad \mathbf{J}_t = \left[ \frac{\partial \mathbf{x}_t}{\partial \mathbf{r}} \right] = \left[ \sum_{i=1}^{nen} \frac{\partial N_i}{\partial \mathbf{r}} (\mathbf{x}_i + t \mathbf{v}_{x_i}) \right],$$

$$\mathbf{J}' = \frac{d\mathbf{J}_t}{dt} = \left[ \sum_{i=1}^{nen} \frac{\partial N_i}{\partial \mathbf{r}} \mathbf{v}_{x_i} \right] = \begin{bmatrix} J'_{11} & J'_{12} & J'_{13} \\ J'_{21} & J'_{22} & J'_{23} \\ J'_{31} & J'_{32} & J'_{33} \end{bmatrix}, \quad (26)$$

$$\begin{aligned} \mathbf{J}' = & J'_{11}(J_{22}J_{33} - J_{23}J_{32}) + J'_{12}(J_{23}J_{31} - J_{21}J_{33}) + J'_{13}(J_{21}J_{32} - J_{22}J_{31}) + J'_{21}(J_{13}J_{32} - J_{12}J_{33}) + J'_{22}(J_{11}J_{33} - J_{13}J_{31}) \\ & + J'_{23}(J_{12}J_{31} - J_{11}J_{32}) + J'_{31}(J_{12}J_{23} - J_{13}J_{22}) + J'_{32}(J_{13}J_{21} - J_{11}J_{23}) + J'_{33}(J_{11}J_{22} - J_{12}J_{21}). \end{aligned} \quad (27)$$

#### 4.3. Traction load sensitivities

As shown in Fig. 9, consider an element in the upstream face of the arch dam that undergoes water pressure. The equivalent nodal forces due to the water pressure are calculated by Eq. (28):

$$\mathbf{P}_s = - \int_{-1}^1 \int_1^1 \mathbf{N}^T \bar{t} \mathbf{A} dr ds = - \sum_{i=1}^{Nquad} w_i \mathbf{N}^T \bar{t} \mathbf{A} \rightarrow \mathbf{P}_s^i = - \sum_{i=1}^{Nquad} w_i N_i \bar{t}_i \mathbf{A}_i,$$

$$\bar{t} = \sum_{i=1}^{nen} N_i t_i : t_i = (h - z_i) \gamma_w. \quad (28)$$

Here  $h$  is the water level,  $z_i$  the water level of node  $i$  and  $\gamma_w$  the weight specific of water. The definitions of other parameters are as follows:

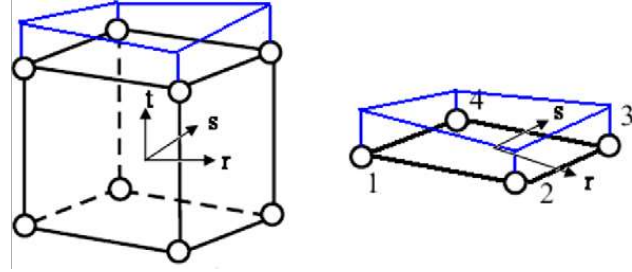


**Fig. 9.** Schematic elements in for traction and its sensitivity calculations.

$$\mathbf{N} = \{N_1, N_2, N_3, N_4\}, \mathbf{A}^T = \left\{ \frac{1}{4} \sum_{i=1}^{nen} N_i \alpha_i \quad \frac{1}{4} \sum_{i=1}^{nen} N_i \beta_i \quad \frac{1}{4} \sum_{i=1}^{nen} N_i \gamma_i \right\}, \quad (29)$$

$$\begin{aligned} \alpha_1 &= y_{12}z_{14} - y_{14}z_{12}, & \alpha_2 &= y_{12}z_{23} - y_{23}z_{12}, \\ \alpha_3 &= y_{34}z_{32} - y_{32}z_{34}, & \alpha_4 &= y_{34}z_{41} - y_{41}z_{34}, \\ \beta_1 &= x_{14}z_{12} - x_{12}z_{14}, & \beta_2 &= x_{23}z_{12} - x_{12}z_{23}, \\ \beta_3 &= x_{32}z_{34} - x_{34}z_{32}, & \beta_4 &= x_{41}z_{34} - x_{34}z_{41}, \\ \gamma_1 &= x_{12}y_{14} - x_{14}y_{12}, & \gamma_2 &= x_{12}y_{23} - x_{23}y_{12}, \\ \gamma_3 &= x_{34}y_{32} - x_{32}y_{34}, & \gamma_4 &= x_{34}y_{41} - x_{41}y_{34}. \end{aligned} \quad (30)$$

The sensitivity of the traction loads is as Eq. (31):

$$\begin{aligned} \mathbf{P}_s^j &= \sum_{i=1}^{N_{quad}} w_i N_i \bar{t}_i \mathbf{A}', \\ \mathbf{A}'^T &= \{A_x \quad A_y \quad A_z\}' = \left\{ \frac{1}{4} \sum_{i=1}^4 N_i \alpha'_i \quad \frac{1}{4} \sum_{i=1}^4 N_i \beta'_i \quad \frac{1}{4} \sum_{i=1}^4 N_i \gamma'_i \right\}, \end{aligned} \quad (31)$$

$$\begin{aligned} \alpha'_1 &= y_{12}V_{z_{14}} + z_{14}V_{y_{12}} - y_{14}V_{z_{12}} - z_{12}V_{y_{14}}, \\ \alpha'_2 &= y_{12}V_{z_{23}} + z_{23}V_{y_{12}} - y_{23}V_{z_{12}} - z_{12}V_{y_{23}}, \\ \alpha'_3 &= y_{34}V_{z_{32}} + z_{32}V_{y_{34}} - y_{32}V_{z_{34}} - z_{34}V_{y_{32}}, \\ \alpha'_4 &= y_{34}V_{z_{41}} + z_{41}V_{y_{34}} - y_{41}V_{z_{34}} - z_{34}V_{y_{41}}, \end{aligned} \quad (32)$$

$$\begin{aligned} \beta'_1 &= x_{14}V_{z_{12}} + z_{12}V_{x_{14}} - x_{12}V_{z_{14}} - z_{14}V_{x_{12}}, \\ \beta'_2 &= x_{23}V_{z_{12}} + z_{12}V_{x_{23}} - x_{12}V_{z_{23}} - z_{23}V_{x_{12}}, \\ \beta'_3 &= x_{32}V_{z_{34}} + z_{34}V_{x_{32}} - x_{32}V_{z_{32}} - z_{32}V_{x_{34}}, \\ \beta'_4 &= x_{41}V_{z_{34}} + z_{34}V_{x_{41}} - x_{34}V_{z_{41}} - z_{41}V_{x_{34}}, \end{aligned} \quad (33)$$

$$\begin{aligned} \gamma'_1 &= x_{12}V_{y_{14}} + y_{14}V_{x_{12}} - x_{14}V_{y_{12}} - y_{12}V_{x_{14}}, \\ \gamma'_2 &= x_{12}V_{y_{23}} + y_{23}V_{x_{12}} - x_{23}V_{y_{12}} - y_{12}V_{x_{23}}, \\ \gamma'_3 &= x_{34}V_{y_{32}} + y_{32}V_{x_{34}} - x_{32}V_{y_{34}} - y_{34}V_{x_{32}}, \\ \gamma'_4 &= x_{34}V_{y_{41}} + y_{41}V_{x_{34}} - x_{41}V_{y_{34}} - y_{34}V_{x_{41}}. \end{aligned} \quad (34)$$

In which  $\mathbf{X}_{ij} = \mathbf{X}_j - \mathbf{X}_i$ ,  $\mathbf{V}_{X_{ij}} = \mathbf{V}_{X_j} - \mathbf{V}_{X_i}$ .

#### 4.4. Stiffness and mass matrixes gradients

After discretization, stiffness matrix for an element is as Eq. (35). The sensitivities of this matrix and its components can be calculated according to the following equations:

$$\mathbf{k}_e = \int_{\Omega} \mathbf{B}^T \mathbf{D} \mathbf{B} d\Omega = \int_{-1}^1 \int_{-1}^1 \int_{-1}^1 \mathbf{B}^T \mathbf{D} \mathbf{B} |\mathbf{J}| dr ds dt = \sum_{i=1}^{N_{quad}} w_i \mathbf{B}^T \mathbf{D} \mathbf{B} |\mathbf{J}|, \quad (35)$$

$$\mathbf{k}'_e = \frac{\partial \mathbf{k}_e}{\partial \mathbf{X}} = \sum_{i=1}^{N_{quad}} w_i (\mathbf{B}^T \mathbf{D} \mathbf{B} |\mathbf{J}| + \mathbf{B}^T \mathbf{D} \mathbf{B}' |\mathbf{J}| + \mathbf{B}^T \mathbf{D} \mathbf{B} |\mathbf{J}'|), \quad (36)$$

$$\mathbf{B}_i^T = \begin{bmatrix} N_{i,x} & 0 & 0 & N_{i,y} & 0 & N_{i,z} \\ 0 & N_{i,y} & 0 & N_{i,x} & N_{i,z} & 0 \\ 0 & 0 & N_{i,z} & 0 & N_{i,y} & N_{i,x} \end{bmatrix}, \quad \mathbf{B}'_i^T = \begin{bmatrix} N'_{i,x} & 0 & 0 & N'_{i,y} & 0 & N'_{i,z} \\ 0 & N'_{i,y} & 0 & N'_{i,x} & N'_{i,z} & 0 \\ 0 & 0 & N'_{i,z} & 0 & N'_{i,y} & N'_{i,x} \end{bmatrix}, \quad (37)$$

$$\frac{\partial N_i}{\partial \mathbf{X}} = \mathbf{J}^{-T} \frac{\partial N_i}{\partial \mathbf{r}} \rightarrow \left( \frac{\partial N_i}{\partial \mathbf{X}} \right)' = -\mathbf{J}^{-T} \mathbf{J}^T \mathbf{J}^{-T} \frac{\partial N_i}{\partial \mathbf{r}} \rightarrow \mathbf{N}'_{i,x} = -\mathbf{J}^{-T} \mathbf{J}^T \frac{\partial N_i}{\partial \mathbf{X}}. \quad (38)$$

Mass matrix formula and its sensitivities are found as follows:

$$\begin{aligned} \mathbf{m}_{ij}^e &= \int_{\Omega} \rho \mathbf{N}^T \mathbf{N} d\Omega = \int_{-1}^1 \int_{-1}^1 \int_{-1}^1 \rho \mathbf{N}^T \mathbf{N} |\mathbf{J}| dr ds dt = \sum_{i=1}^{N_{quad}} w_i \rho \mathbf{N}^T \mathbf{N} |\mathbf{J}|, \\ \mathbf{m}'_{ij}^e &= \sum_{i=1}^{N_{quad}} w_i \rho \mathbf{N}^T \mathbf{N} |\mathbf{J}|'. \end{aligned} \quad (39)$$

#### 4.5. Sensitivities of seismic loadings

In response spectrum method, the maximum nodal displacements and stresses of elements are computed separately for each individual mode of vibration and then combined to obtain the total maximum response. The responses and sensitivities are calculated as:

$$\mathbf{M} \ddot{\mathbf{U}} + \mathbf{C} \dot{\mathbf{U}} + \mathbf{K} \mathbf{U} = \mathbf{P} : \mathbf{U} = \Phi \mathbf{y}, \quad (40)$$

$$\frac{\partial \mathbf{U}}{\partial \mathbf{X}} = \sum_{n=1}^{n_{mod}} \left( \frac{\partial \Phi_n}{\partial \mathbf{X}} y_n + \Phi_n \frac{\partial y_n}{\partial \mathbf{X}} \right). \quad (41)$$

Consider,  $\mathbf{K} \Phi_n = \lambda_n \mathbf{M} \Phi_n$ ,  $\Phi_n^T \mathbf{M} \Phi_n = \mathbf{I}$ , and differentiating with respect to the design variables, the sensitivities of eigenvalues are as:

$$\frac{\partial \lambda_n}{\partial \mathbf{X}} = \left( \Phi_n^T \left( \frac{\partial \mathbf{K}}{\partial \mathbf{X}} - \lambda_n \frac{\partial \mathbf{M}}{\partial \mathbf{X}} \right) \Phi_n \right) / M_n. \quad (42)$$

The results show that, the sensitivities of eigenvectors have trivial effects on the dynamic responses [32]

$$\ddot{y}_n + 2\xi_n \omega_n \dot{y}_n + \omega_n^2 y_n = \Phi_n^T \mathbf{P} \rightarrow y_n = \frac{L_n}{M_n \lambda_n} S_{an}(T_n, \xi_n), \quad (43)$$

where  $L_n$ ,  $M_n$ ,  $S_{an}$  and  $T_n$  are modal load, modal mass, spectral acceleration and period for mode  $n$ , respectively. The design dependent loading derivatives in the response spectrum method are calculated as:

$$\begin{aligned} \frac{\partial y_n}{\partial \mathbf{X}} &= \frac{\partial L_n}{\partial \mathbf{X}} \cdot \frac{S_{an}}{M_n \lambda_n} - \frac{L_n S_{an}}{M_n^2 \lambda_n^2} \cdot \frac{\partial M_n}{\partial \mathbf{X}} - \frac{L_n S_{an}}{M_n \lambda_n^2} \cdot \frac{\partial \lambda_n}{\partial \mathbf{X}} + \frac{L_n}{M_n \lambda_n} \cdot \frac{\partial S_{an}}{\partial \mathbf{X}}, \\ \frac{\partial L_n}{\partial \mathbf{X}} &= \frac{\partial \Phi_n^T}{\partial \mathbf{X}} \mathbf{M} \{1\} + \Phi_n^T \frac{\partial \mathbf{M}}{\partial \mathbf{X}} \{1\}, \quad \frac{\partial S_{an}}{\partial \mathbf{X}} = g\left(\frac{\partial \lambda_n}{\partial \mathbf{X}}\right), \quad \lambda_n = \omega_n^2. \end{aligned} \quad (44)$$

Here  $g$  is a function. One might assume a polynomial fit for the above response spectrum, e.g.  $S_{an} = a\omega_n^3 + b\omega_n^2 + c\omega_n + d$ .

#### 4.6. Sensitivities of stresses

Principal stresses ( $\bar{\sigma}_e$ ) calculation for a three-dimensional solid can be numerically evaluated from the stresses ( $\sigma_e$ ) in the xyz coordinate system by solving a cubic equation. An alternative approach to this problem is to write the basic stress transformation equation in terms of the unknown directions of the principal stresses ( $\theta$ ) in the 1-2-3 reference system as Eq. (45):

$$\bar{\sigma}_e = \theta^T \sigma_e \theta : \begin{bmatrix} \sigma_1 & 0 & 0 \\ 0 & \sigma_1 & 0 \\ 0 & 0 & \sigma_1 \end{bmatrix} = \begin{bmatrix} \theta_{x1} & \theta_{y1} & \theta_{z1} \\ \theta_{x2} & \theta_{y2} & \theta_{z2} \\ \theta_{x3} & \theta_{y3} & \theta_{z3} \end{bmatrix} \begin{bmatrix} \sigma_{xx} & \sigma_{xy} & \sigma_{xz} \\ \sigma_{yx} & \sigma_{yy} & \sigma_{yz} \\ \sigma_{zx} & \sigma_{zy} & \sigma_{zz} \end{bmatrix} \begin{bmatrix} \theta_{x1} & \theta_{x2} & \theta_{x3} \\ \theta_{y1} & \theta_{y2} & \theta_{y3} \\ \theta_{z1} & \theta_{z2} & \theta_{z3} \end{bmatrix}. \quad (45)$$

In which  $\theta$  is the standard direction cosine matrix. Sensitivities of stresses ( $\sigma'_e$ ) at gauss or nodal points are calculated as in Eq. (46):

$$\sigma'_e = \frac{\partial \sigma_e}{\partial \mathbf{X}} = \mathbf{D} \frac{\partial \mathbf{B}}{\partial \mathbf{X}} \mathbf{u}_e + \mathbf{D} \mathbf{B} \frac{\partial \mathbf{u}_e}{\partial \mathbf{X}}. \quad (46)$$

Usually, the values of  $\sigma'_1$ ,  $\sigma'_2$ ,  $\sigma'_3$  or the derivatives of the principal stresses are needed. The sensitivities of  $\bar{\sigma}'_e$  are computed as Eq. (47):

$$\bar{\sigma}'_e = \theta^T \sigma_e \theta + \theta^T \sigma'_e \theta + \theta^T \sigma_e \theta'. \quad (47)$$

In CQC method, maximum stresses calculated as:

$$\sigma_{\max} = \sqrt{\sum_{m=1}^P \sum_{n=1}^P \sigma_m \rho_{mn} \sigma_n}. \quad (48)$$

Here  $P$  is the number of vibration modes, and  $\rho_{mn}$  is a component of the cross-modal matrix. The derivatives of stresses in response spectrum method can be computed as follows:

$$\sigma'_{\max} = \frac{\partial \sigma_{\max}}{\partial \mathbf{X}} = \left( \sum_{m=1}^P \sum_{n=1}^P (\sigma'_m \rho_{mn} \sigma_n + \sigma_m \rho'_{mn} \sigma_n + \sigma_m \rho_{mn} \sigma'_n) \right) / 2 \sqrt{\sum_{m=1}^P \sum_{n=1}^P (\sigma_m \rho_{mn} \sigma_n)}, \quad (49)$$

$$\begin{aligned} \rho_{mn} &= 8\xi^2(1+r)r^3/((1-r^2)^2 + 4\xi^2r(1+r)^2) = a/b : r = \frac{T_m}{T_n} \rightarrow \rho'_{mn} = (a'b - ab')/b^2, \\ a' &= 8\xi^2r'r^3 + 12\xi^2r'(1+r)r^{\frac{1}{2}}, \quad b' = -4r'r(1-r^2) + 8\xi^2rr'(1+r). \end{aligned} \quad (50)$$

In which,  $T_m$  is the period of  $m$ th mode of vibration.

## 5. Optimization

### 5.1. Design variables

The shape of arch dam and abutments can be created using the declared design variables in Section 2 (Fig. 7). The Design variables are expressed in the array  $\mathbf{X} = \{\bar{\mathbf{X}}_1, \bar{\mathbf{X}}_2, \bar{\mathbf{X}}_3, \bar{\mathbf{X}}_4, \bar{\mathbf{X}}_5, \bar{\mathbf{X}}_6\}$ . Here  $\bar{\mathbf{X}}_1 = \{p_c, p_u, p_m, p_b\}$  denotes the overhang parameters of the crown cantilever at the four reference elevations.  $\bar{\mathbf{X}}_2 = \{T_c, T_u, T_m, T_b\}$  shows the thicknesses of a crown cantilever,  $\bar{\mathbf{X}}_3 = \{R_c, R_u, R_m, R_b\}$  describes the radiiuses of curvature of the arch parabola vertex,  $\bar{\mathbf{X}}_4 = \{T_{cr}, T_{ur}, T_{mr}, T_{br}, T_{cl}, T_{ul}, T_{ml}, T_{bl}\}$  the thicknesses of right and left abutments,  $\bar{\mathbf{X}}_5 = \{\mathbf{t}_c, \mathbf{t}_u, \mathbf{t}_m, \mathbf{t}_b, \mathbf{s}_c, \mathbf{s}_u, \mathbf{s}_m, \mathbf{s}_b\}$  the right and the left starting points of variable thickness arches. The entire latter are expressed in the four reference elevations (as the interpolation stations).  $\bar{\mathbf{X}}_6 = \{d_{cr}, d_{ur}, d_{mr}, d_{cl}, d_{ul}, d_{ml}, d_b\}$  indicates the excavation depths at the left and the right abutments and at the crown cantilever base.

### 5.2. Objective function

Usually, the objective function is the costs of the dam body concrete. However, here, the total volume of the foundation excavation and the dam volume is used as Eq. (51):

$$F(\mathbf{X}) = V_{\text{dam}}(\mathbf{X}) + V_{\text{exc}}(\mathbf{X}), \quad (51)$$

where  $F(\mathbf{X})$  is the objective function,  $V_{\text{dam}}(\mathbf{X})$  is the volume of concrete in the dam body,  $V_{\text{exc}}(\mathbf{X})$  is the volume of foundation excavation, and  $\mathbf{X}$  is the vector of design variables.

### 5.3. Constraints

In shape optimization of concrete arch dams, the following three types of constraint sets should be satisfied as required by the demands of design and construction:

- (1) geometrical constraints set,
- (2) stress constraints set,
- (3) stability constraints set.

All the constraints of these sets are expressed in the form of  $g_j(\mathbf{X}) \leq 0$  in the optimization problem. In this study, the stability constraints set is not considered.

#### 5.3.1. Geometrical constraints

To facilitate the construction, the maximum value of the overhang slope at the upstream and downstream faces ( $\theta_{CU}$  and  $\theta_{BD}$ ), as well as the maximum overhang at the upstream face relative to the toe (Undercut) should be limited by Eq. (52), as shown in Fig. 10. Furthermore, the Hermite splines at elevation  $H_u$  of the upstream face should have a positive curvature, as in Eq. (52):

$$\begin{aligned} \theta_{CU} &\leq \theta_{C\max}, \quad \theta_{BD} \leq \theta_{B\max}, \\ \text{Undercut} &\leq U_{alw}, \quad y''_U \geq 0. \end{aligned} \quad (52)$$

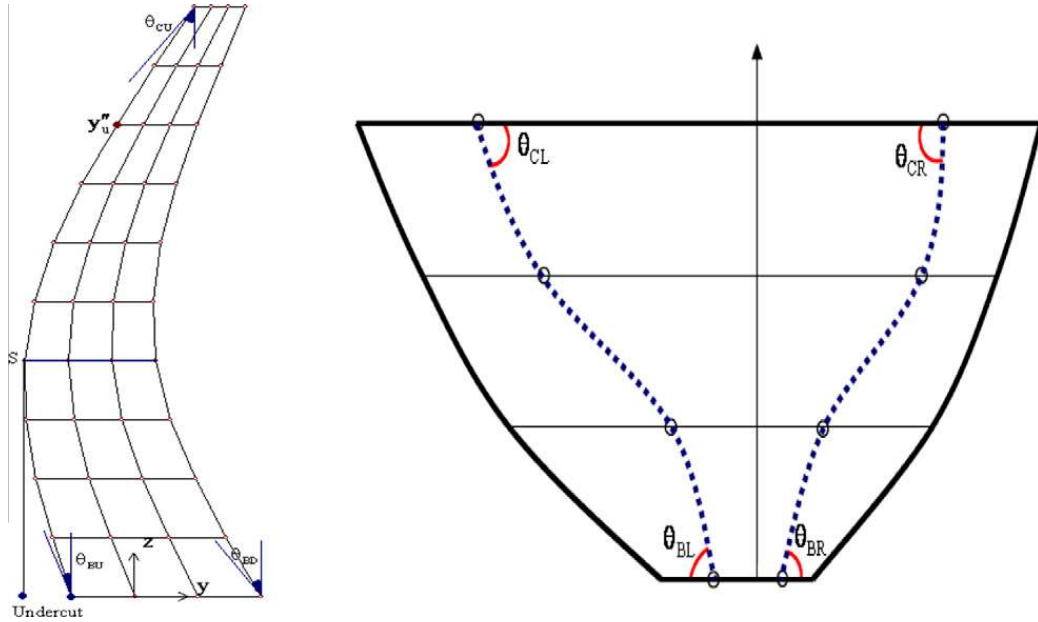


**Fig. 10.** Slope of overhangs (left) & intersection angle of variable thickness starting limit with the crest and bottom arches (right).

For constructing purposes and to guarantee the smoothness of cantilevers over the dam height, the boundaries of variable thickness zones must satisfy Eq. (53):

$$\begin{aligned} \theta_{CR}, \quad |\theta_{CL}| &\geq \bar{\theta}_C, \\ \theta_{BR}, \quad |\theta_{BL}| &\geq \bar{\theta}_B, \end{aligned} \quad (53)$$

where  $\theta_{B\max}$ ,  $\theta_{C\max}$ ,  $U_{alw}$  and  $\bar{\theta}_C$ ,  $\bar{\theta}_B$  are the allowable values of the aforementioned parameters. According to the requirements of traffic and the access to the equipments located at different points of the dam crest, its minimum thickness is as well decided. The maximum thickness of the base of the dam could be also limited.

$$T_c \geq (T_c)_{\min}, \quad T_b \leq (T_b)_{\max}. \quad (54)$$

**Table 1**

Stress constraints used in the loading cases [33].

Loading case 1 (separate cantilevers)	Loading case 1 (monolithic body)	Loading case 2	Loading case 3
$(\sigma_{ti})_{\text{heel}} \leq 0.10f_{cc}$	$\sigma_{ti} \leq 0.05f_{cc}$	$\sigma_{ti}^{\text{st}} \leq 0.50 \text{ MPa}$	$\sigma_{ti}^{\text{dy}} \leq 0.65f_{cc}^{2/3}$
$ (\sigma_{ci})_{\text{toe}}  \leq 0.25f_{cc}$	$ \sigma_{ci}  \leq 0.25f_{cc}$	$ \sigma_{ci}^{\text{st}}  \leq 0.33f_{cc}$	$ \sigma_{ci}^{\text{dy}}  \leq 1.30f_{cc}$

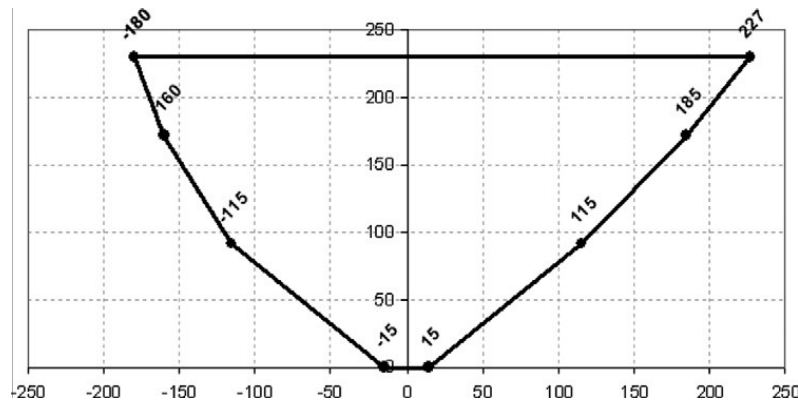


**Fig. 11.** Karun IV valley shape, with its left and right widths values ( $L_{ir}, L_{il}$ ).

### 5.3.2. Stress constraints

In shape optimization of arch dams, several types of stresses should be considered as constraints. In accordance with the required safety factors in each loading case, and the type of stress component, the constraints could be defined in terms of allowable tensile and compressive stresses in the free standing cantilevers, or on the upstream and downstream faces of monolithic shell structure. The allowable shear stress at cantilevers lift joints is also taken as a constraint. The stress constraints used for the three loading cases in this work have been summarized as in Table 1. Here  $\sigma_{ci}$ ,  $\sigma_{ti}$  are the maximum and minimum principal stresses in each load case at the Gauss points in solid elements of the dam body at air and water surfaces except for case 3 in which these stresses corresponds to the arch and cantilever directions.  $f_{cc}$  is the uniaxial compressive strength of concrete at the age of ninety days. Subscripts  $st$  and  $dy$  stand for the total stresses in static or dynamic cases. Control of shear stresses in the cantilevers and in the monolithic structure in loading cases 2, and 3 has an important role in arch dam design. Shear stresses in horizontal lift joints should satisfy the following equations according to the Mohr–Coulomb failure criterion.

$$\tau_{\max} \leq \tau_{\text{alw}}, \quad \tau_{\text{alw}} = -\sigma_n + c \tan \phi. \quad (55)$$

**Table 2**

Dam height and material properties.

Height (m)	$f_{cc}$ (Mpa)	$E_c$ (Gpa)	$E_r$ (Gpa)	$\gamma_c$ (kN/m <sup>3</sup> )	$v_c$	$v_r$
230	35	22	8	24	.18	.22

**Table 3**

Allowable value of geometry constraints.

$T_{\min}(m)$	$T_{\max}(m)$	$\theta_{B\max}$	$\theta_{C\max}$	$U_{\text{alw}}(m)$	$\bar{\theta}_B$	$\bar{\theta}_C$
6.5	0.25H	20°	20°	6.0	70°	70°

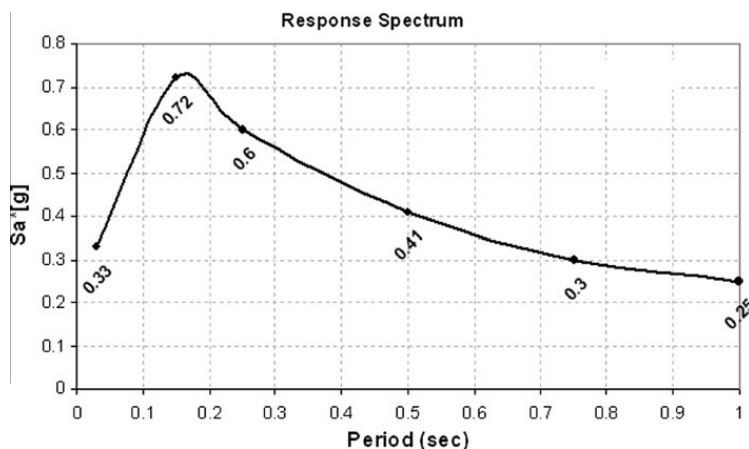


**Fig. 12.** Seismic response spectrum used for dam site for longitudinal direction.

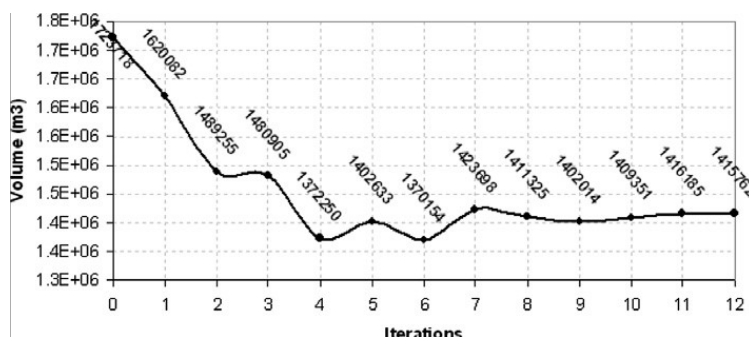


**Fig. 13.** The convergence rate of the objective function.

#### 5.4. Optimization method

Arch dam shape optimization problem can now be expressed in a nonlinear constrained optimization problem as:

$$\begin{aligned} & \text{minimize : } F(\mathbf{X}) \\ & \text{subject to :} \\ & g_j(\mathbf{X}) \leq 0, \quad j = 1, 2, \dots, m, \\ & \mathbf{X}^L \leq \mathbf{X} \leq \mathbf{X}^U. \end{aligned} \quad (56)$$

Here  $F(\mathbf{X})$  is the objective function,  $\mathbf{X}_U$ , and  $\mathbf{X}_L$  the upper and the lower bounds of the vector of design variables, and  $m$  is the total number of constraints. Direct solution of Eq. (56) is prohibitive because of the computational costs of the structure and the sensitivities analysis at each iteration of the optimization procedure. To solve Eq. (56), The SQP algorithm is used to carry

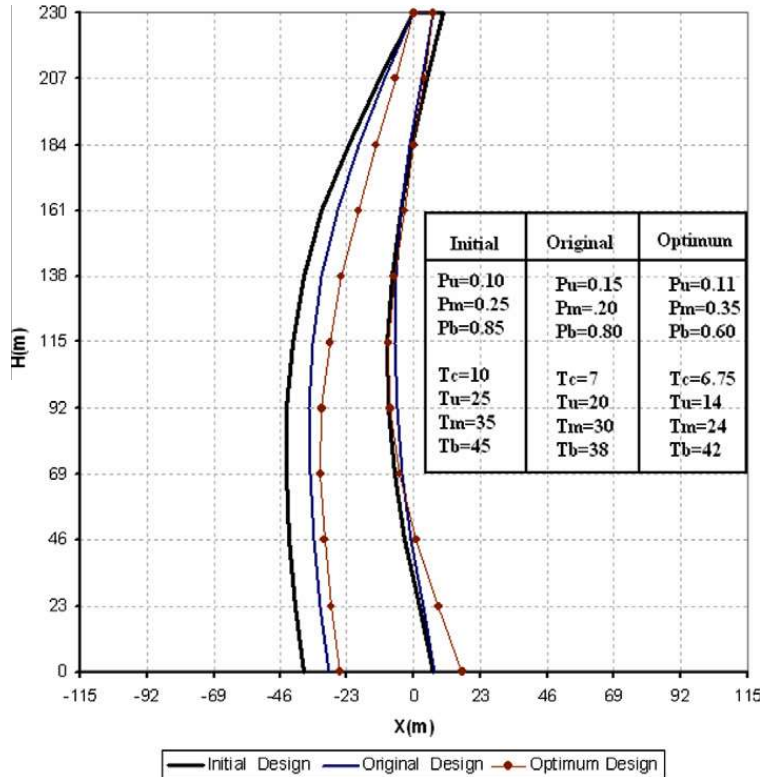


Fig. 14. Shape of the crown cantilever in the initial, original and optimum designs.

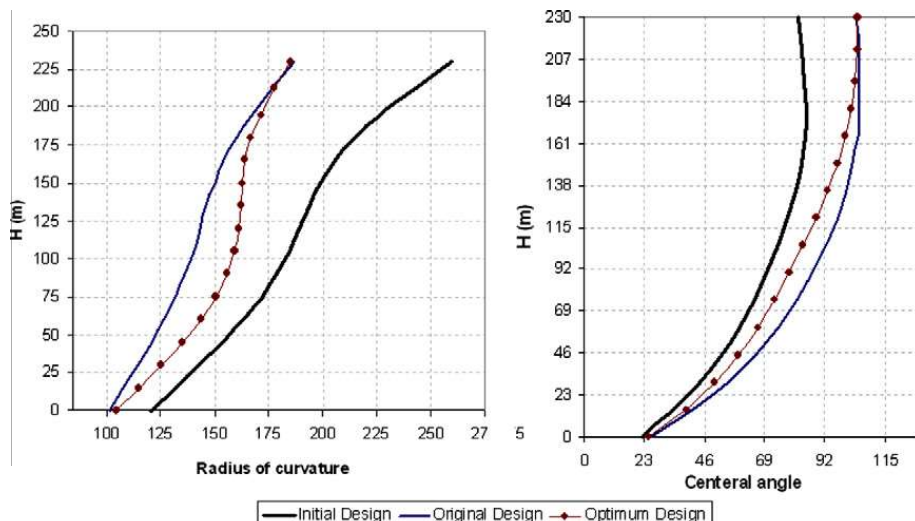


Fig. 15. Variation of the curvature radii and central angle versus the height.

out a “direction finding”. Because of the wide range of the design variables, the design variables are normalized to increase the rate of convergence as:

$$\mathbf{X}' = \frac{\mathbf{X}}{\mathbf{X}_0} \rightarrow X'_i = \frac{X_i}{X_{0i}}. \quad (57)$$

## 6. Test cases

The algorithms described above are applied to the shape optimization of the Karun IV concrete arch dam located in Khuzestan province in south of Iran. The dam has been constructed in a valley site as shown in Fig. 11. The dam concrete and rock major properties (compressive strength, modulus of elasticity, specific gravity, poisson ratio), and the main geometrical

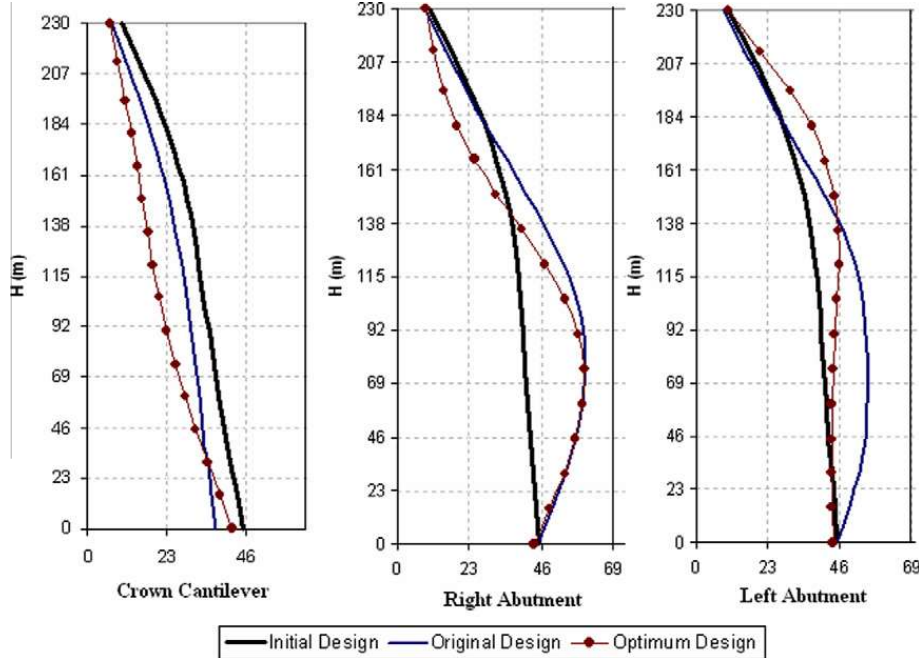


**Fig. 16.** Variation of the thickness profiles for the crown and abutments versus the height.

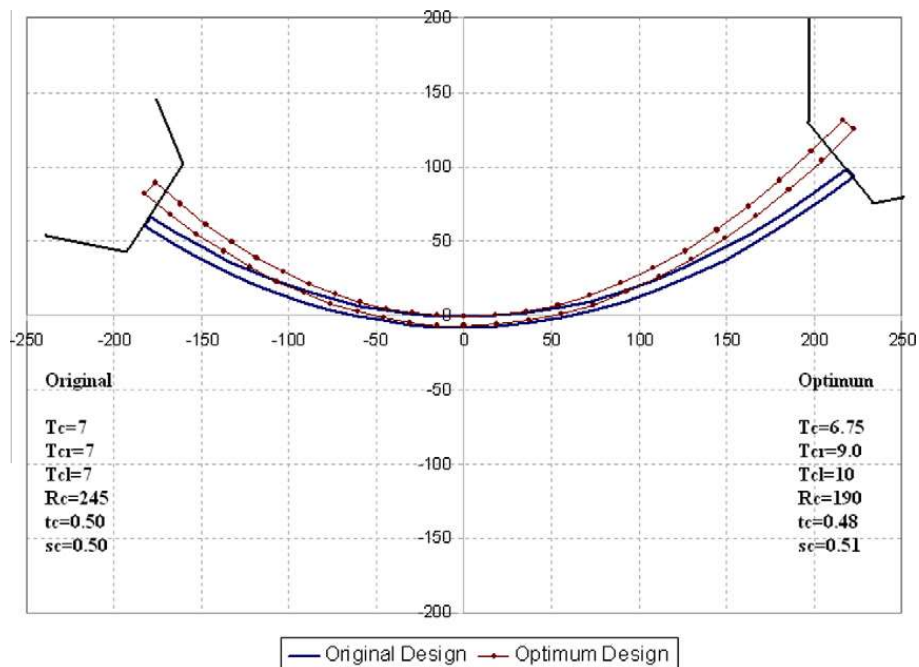


**Fig. 17.** Geometrical specifications of the horizontal arch for the original and the optimum designs at crest.

constraint values used for the shape optimization process, are described in **Tables 2 and 3**. Here subscripts r and c stand for rock and concrete. In load case 3, the concrete compressive strength and modulus of elasticity values are increased by a factor of 1.33.

The seismic input load for the shape optimization is based on the level actually used for the design of this dam. Here only longitudinal component of its acceleration response spectrum (**Fig. 12**) has been considered as the target seismic input.

### 6.1. Numerical results

The shape optimization of the Karun-IV arch dam according to the above methodologies converged after 12 iterations. The costs of sensitivities in this paper are about (3%) of the costs of the forward or backward finite difference based gradient

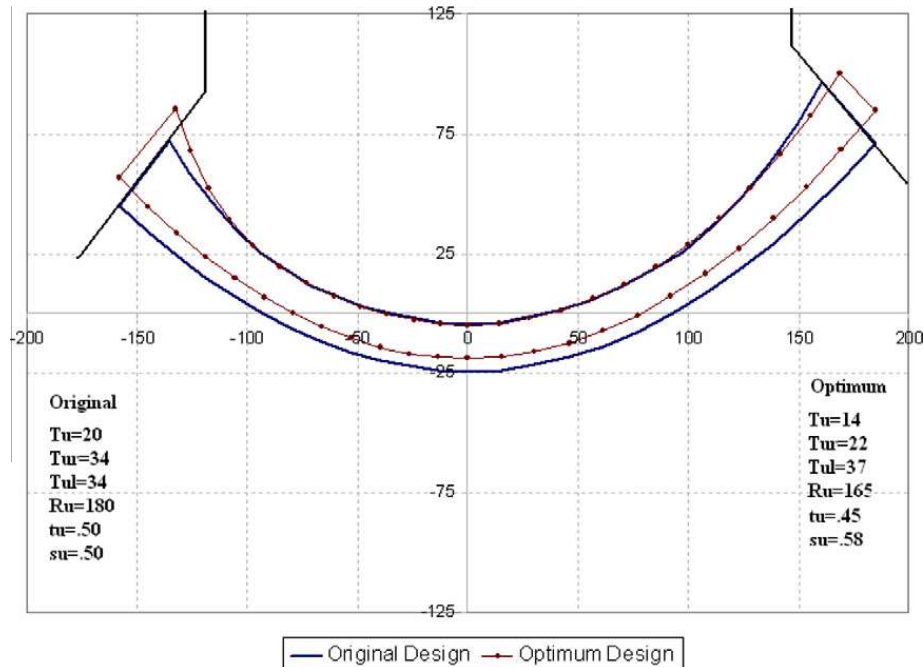


**Fig. 18.** Geometrical specifications of the horizontal arch for the original and the optimum designs at  $H_U$ .

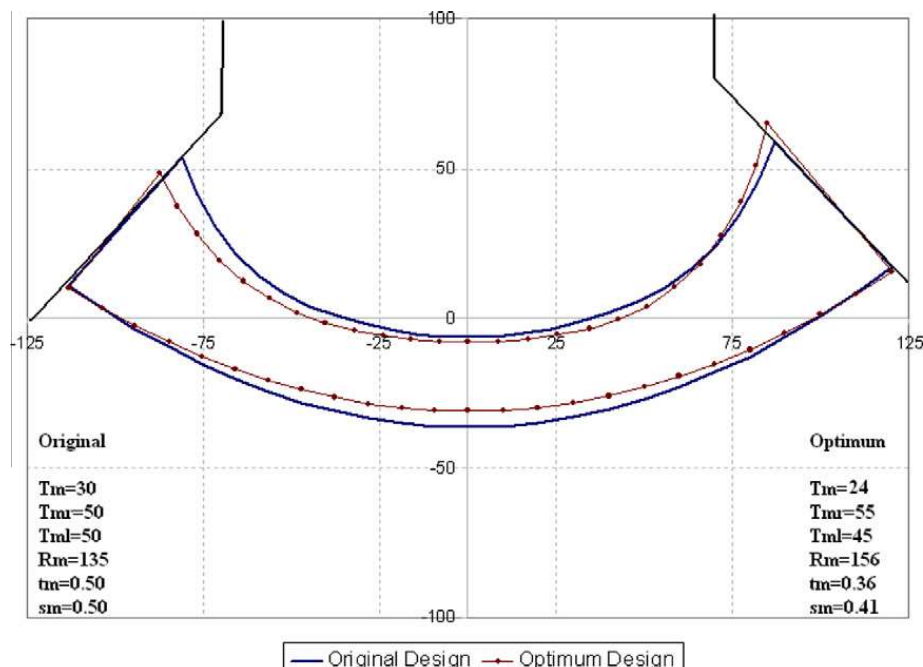


**Fig. 19.** Geometrical specifications of the horizontal arch for the original and the optimum designs at  $H_m$ .

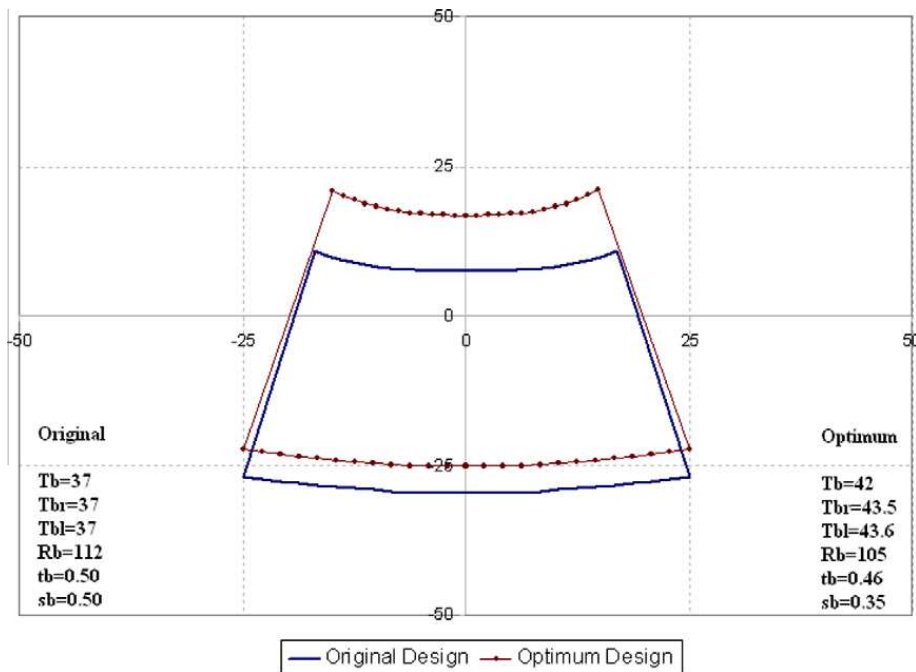


**Fig. 20.** Geometrical specifications of the horizontal arch for the original and the optimum designs at bottom.

calculations methods. To calculate the sensitivities with the finite difference based methods, the full finite element analysis has to be performed for each design variable. Therefore, for 34 design variables, 34 times the full finite element analysis is required, but in the proposed finite element based sensitivity analysis method, only one full finite element analysis is needed. Consequently, the cost of computations of nominated method is  $(1/34)*100$  or (3%) of the cost of classical approaches. Furthermore, the accuracy of the derivatives in the finite difference methods depends on the perturbation of the design variables ( $\Delta X_i$ ), whereas in the proposed method the accuracy of gradients is independent of the perturbation values. The convergence rate of the objective function in the optimization process is illustrated in Fig. 13. As well, Fig. 14 shows the initial, the original and the optimum shapes. After performing the optimization process, the dam and excavation volume has decreased by (18%) in comparison with the initial design, and (10%) in comparison with the original design. In Fig. 15–20, the optimization results of this arch dam have been illustrated.

## 7. Conclusion

This paper employs an organized methodology to find the optimum shape of arch dams. In order to create the geometry of arch dams a new algorithm based on Hermit Splines is proposed. A finite element based shape design sensitivity involving body force, hydrostatic pressure and earthquake loadings is accomplished. The sensitivity analysis is represented using the concept of mesh design velocity. The cost of sensitivity analysis in this paper is about (3%) of the cost of the forward or backward finite difference based gradient calculation methods. Moreover, the accuracy of the derivatives in the finite difference methods depends on the perturbation of the design variables ( $\Delta X_i$ ), whereas in this paper the accuracy of sensitivities is independent of perturbation values. In the optimization model, many geometrical and behavioral constrains are included in the model in comparison with previous researches.

## Acknowledgments

Authors wish to express their gratitude to the Water Resource Management Company-Ministry of Energy of Iran for the financial supports of this project. The first author would like to express his gratitude to Professor R.L. Taylor emeritus professor of Berkeley University in California and N.H. Kim associate professor of University of Florida for their ideas and encouragements.

## References

- [1] J.F.L. Fialho, Leading Principles for the Design of Arch Dams – A New Method of Tracing and Dimensioning, LNEC, Lisbon, Portugal, 1955.
- [2] J.L. Serafim, New shapes for arch dams, Civil Engineering, ASCE 36 (2) (1966).
- [3] M.K.S. Rajan, Shell Theory Approach for Optimization of Arch Dam Shapes, Ph.D Thesis, University of California, Berkeley, 1968.
- [4] G.A. Mohr, Design of shell shape using finite elements, Comput. Struct. 10 (5) (1979) 745–749.
- [5] R.L. Sharma, Optimal Configuration of Arch Dams, Ph.D Thesis, Indian Institute of Technology, Kanpur, 1983.
- [6] R. Sharpe, The optimum design of arch dams, in: Proceeding of Institution of Civil Engineers (ICE), 1969, Paper. 7200s, Suppl Vol., pp. 73–98.

- [7] R.E. Ricketts, O.C. Zienkiewicz, Shape optimization of concrete dams, Criteria and Assumptions for Numerical Analysis of Dams, Quadrant Press, Swansea, London, UK, 1975. pp.1179–1206.
- [8] K. Wassermann, Three dimensional shape optimization of arch dams with prescribed shape functions, *J. Struct. Mech.* 11 (4) (1984) 465–489.
- [9] A.S. Rahim, Optimum Shape of An Arch Dam for Static Loads, MEng Thesis, Asian Institute of Technology, Bangkok, 1983.
- [10] M.S. Samy, M. Wieland, Shape optimization of arch dams for static and dynamic loads, in: Proceedings of International Workshop on Arch Dams, Coimbra, 1987.
- [11] T.M. Yao, K.K. Choi, Shape optimal design of an arch dam, *J. Struct. Eng., ASCE* 115 (9) (1989) 2401–2405.
- [12] L. Guohua, W. Shuyu, Optimum design of concrete arch dam, *Proc. Int. Concrete Conf.*, Tehran (1990) 444–452.
- [13] A. Fanelli, M. Fanelli, P. Salvaneschi, A neural network approach to the definition of near optimal arch dam shape, *Dam Eng. IV* (2) (1993) 123–140.
- [14] M. Maher, N.T. Bidokhti, shape optimization of concrete arch dams using simple genetic algorithm, *Dam Eng. XIV* (2) (2001).
- [15] J. Salajegheh, E. Salajegheh, S.M. Seyedpoor, S. Golizadeh, Optimum design of arch dams including hydrodynamic effects for earthquake loading using the simultaneous perturbation stochastic approximation method, in: B.H.V. Topping, M. Papadrakakis (Eds.), Proceedings of the Ninth International Conference on Computational Structures Technology, Civil-Comp Press, Stirlingshire, UK, 2008. Paper 60.
- [16] S.M. Seyedpoor, J. Salajegheh, E. Salajegheh, S. Golizadeh, Optimum shape design of arch dams for earthquake loading using a fuzzy inference system and wavelet neural networks, *Eng. Optim.* 41 (2009) 473–493.
- [17] S.M. Seyedpoor, J. Salajegheh, E. Salajegheh, Shape optimal design of arch dams including dam–water–foundation rock interaction using a grading strategy and approximation concepts, *Appl. Math. Model.* (2009).
- [18] Z. Bofang, Shape optimization of arch dams, *Int. Water Power Dam Construct.* 39 (3) (1987) 43–51.
- [19] Z. Bofang, Optimum design of arch dams, *Dam Eng.* I (2) (1990) 131–145.
- [20] Z. Bofang, B. Rao, J. Jia, Y. Li, Shape optimization of arch dams for static and dynamic loads, *J. Struct. Eng., ASCE* 118 (11) (1992) 2996–3015.
- [21] L.M.C. Simoes, J.A.M. Lapa, Optimal shape of dams subject to earthquakes, in: B.H.V. Topping, M. Papadrakakis (Eds.), *Adv. Struct. Optim.*, Civil-Comp Press, Edinburgh, UK, 1994, pp. 119–130.
- [22] L.M.C. Simões, Shape optimization of dams for static & dynamic loading, *Proc. Int. Conf. Hydroelectric Power Plants*, Coimbra, Portugal (1995) 171–190.
- [23] Li Shouyi, L. Ding, L. Zhao, W. Zhou, Optimization design of arch dam shape with modified complex method, *Adv. Eng. Software* 40 (2009) 804–808.
- [24] Linsong Sun, Dexing Wang, Wenjun Sun, Shape optimization of arch dam subject to crack depth constrain, *J. Hydraulic Eng.* (1998) 10.
- [25] Xiao-fei Zhang, Li Shouyi, Yao-long Chen, Optimization of geometric shape of Xiamen arch dam, *Adv. Eng. Software* 40 (2009) 105–109.
- [26] z. Wu, Y.T. Wang, Fuzzy optimization of arch dams, *Proc. 1st National Conf. Hydraulic Struct. Young Sci. Eng.* (1991) 25–29.
- [27] Nenggan Xie, Dexing Wang, Linsong Sun, Application of energy function on dynamic optimization of high arch dam, *Chinese J. Appl. Mech.* 2 (2000).
- [28] F. Tajalli, M.T. Ahmadi, H. Moharrami, Shape optimization of concrete arch dam to enhance seismic performance, *Dam Eng.* XVIII (2) (2007).
- [29] J. Akbari, M.T. Ahmadi, Shape optimization of concrete arch dams for dynamic loading using mesh design velocity, *Dam Eng.* XX (I) (2009) 77–98.
- [30] J. Akbari, N.H. Kim, M.T. Ahmadi, Shape sensitivity analysis with design-dependent loadings-equivalence between continuum and discrete derivatives, *Struct. Multidisc. Optim.* 40 (1–6) (2010) 353–364.
- [31] K.K. Choi, N.H. Kim, Structural Sensitivity Analysis and Optimization, Springer-Verlag, New York, 2004.
- [32] U. Kirsch, M. Bogomolni, I. Sheinmen, Efficient design sensitivities of structures subjected to dynamic loading, *Int. J. Solid Struct.* 43 (2006) 5485–5500.
- [33] Shahid Rajaei, Dam static and Dynamic Elastic Stress Analysis of Dam Body, Report Mahab-Ghods & Stucky Electro Watt, JV.Tehran, 1994.